Event Horizon Telescope
Memo Series

EHT Memo 2019-CE-03

Calibration & Error Analysis WG

Global calibration of instrumental polarimetric phase gains

S. Steel[1,2,*], M. Wielgus[1,2,†], L. Blackburn[1,2], S. Issaoun[3], M. D. Johnson[1,2]

Jul 9, 2019 – Version 1.0

[1]*Center for Astrophysics | Harvard & Smithsonian, 60 Garden St., Cambridge, MA 02138, USA*
[2]*Black Hole Initiative at Harvard University, 20 Garden St., Cambridge, MA 02138, USA*
[3]*Department of Astrophysics/IMAPP, Radboud University, P.O. Box 9010, 6500 GL Nijmegen, The Netherlands*

Abstract

This memo summarizes formalism describing the polarimetric calibration, focusing on measuring LCP-RCP phase offsets for each station from differences between phases in *LL* and *RR* visibilities on baselines to a reference station. We introduce a new calibration procedure utilizing multiple sources and globally fitting to the phase offsets in order to prevent overfitting to the intrinsic source polarimetric properties. In this procedure we calculate a family of polynomial and piecewise linear fits and select the optimal one using a proper information criterion.

[*]sangersteel@gmail.com
[†]maciek.wielgus@gmail.com

1 Polarimetric calibration formalism

1.1 Principles of interferometry

The quantity measured in a radiointerferometric observation is the mutual coherence Γ of the incoming radiation, between two observing points $\mathbf{r_1}$ and $\mathbf{r_2}$. We denote the electromagnetic field measured by each point (each telescope) as $\mathbf{E_1}$ and $\mathbf{E_2}$ respectively. The mutual coherence function between these two observation points can be written as

$$\Gamma_{12}\left(\tau, \mathbf{r_1}, \mathbf{r_2}\right) = \lim_{T\to\infty} \frac{1}{2T} \int_{-T}^{T} E_1(t)\, E_2^*(t-\tau)\, \mathrm{d}t \tag{1}$$

for τ representing the time offset between the arrival of signal at the two telescopes. T is the averaging time [1, 2]. Once the offset τ is accounted for [3, 4], we can represent the coherence function as the value of correlation between the electromagnetic fields E_1 and E_2,

$$\Gamma_{12} = \langle E_1, E_2^* \rangle\ . \tag{2}$$

We refer to this correlated product as a *visibility function* $\mathcal{V}$. By the Van Cittert-Zernike theorem the visibility function is equivalent to the Fourier transform of the brightness in the sky I, that is

$$\mathcal{V}(u,v) = \iint I(l,m)\, e^{-2\pi i(ul+vm)}\, \mathrm{d}l\, \mathrm{d}m\ . \tag{3}$$

Coordinates (u, v) represent the projection of baseline $\mathbf{r_2} - \mathbf{r_1}$ onto the plane of observations, in the units of wavelength λ. The coordinates l and m are direction cosines to the source measured with respect to the u and v axes. The overarching goal of very long baseline interferometry (VLBI, [1]) as is concerned by the Event Horizon Telescope (EHT) is then to characterize the spatial distribution of the source brightness $I(l, m)$ based on the sparsely sampled Fourier domain data $\mathcal{V}(u, v)$.

1.2 Polarimetric calibration

Polarized emission from the astronomical source may encode important characterization of the magnetic field geometry [5]. A full polarized state of the radiation field can be measured in a VLBI observation by using two receivers, susceptible to orthogonally polarized components. In case of the circular polarization basis measurements, a following relation with the Stokes components [6, 7] is found

$$\begin{pmatrix} \tilde{I}_{1,2} \\ \tilde{Q}_{1,2} \\ \tilde{U}_{1,2} \\ \tilde{V}_{1,2} \end{pmatrix} = \frac{1}{2} \begin{pmatrix} \langle E_{1,R} E_{2,R}^* \rangle + \langle E_{1,L} E_{2,L}^* \rangle \\ \langle E_{1,L} E_{2,R}^* \rangle + \langle E_{1,R} E_{2,L}^* \rangle \\ i\left(\langle E_{1,L} E_{2,R}^* \rangle - \langle E_{1,R} E_{2,L}^* \rangle\right) \\ \langle E_{1,R} E_{2,R}^* \rangle - \langle E_{1,L} E_{2,L}^* \rangle \end{pmatrix} = \frac{1}{2} \begin{pmatrix} \mathcal{V}_{RR} + \mathcal{V}_{LL} \\ \mathcal{V}_{LR} + \mathcal{V}_{RL} \\ i\left(\mathcal{V}_{LR} - \mathcal{V}_{RL}\right) \\ \mathcal{V}_{RR} - \mathcal{V}_{LL} \end{pmatrix}. \tag{4}$$

in which the left hand side of the equation 4 represents Stokes parameters, and the right hand side represents the measured circular polarization components, with indices "R" and "L" denoting right and left circular polarization, respectively. The majority of the EHT array telescopes measure the electric field in a circular basis (with the exception of ALMA, which performs measurement in a linear basis, subsequently converted to a circular basis at the correlation stage [8]). In equation 4, $\tilde{I}_{1,2}$ denotes the Fourier transform of the total intensity of the light I, and the remaining parameters can be thought as degrees to which the light is polarized linearly and circularly. Particularly, Stokes V, is related to the amount of circular polarization. If $\tilde{V} = 0$ then $\mathcal{V}_{RR} = \mathcal{V}_{LL}$, so there is no phase difference between the two. This constitutes an approximation that is useful for the data calibration and in many cases sufficiently accurate, as based on physical motivations we would expect $\tilde{I} > \tilde{Q} \approx \tilde{U} > \tilde{V}$. However, it is scientifically interesting to be able to detect $\tilde{V}$, or at least to put constraints on its magnitude. For that reason in this memo we attempt to relax the $V = 0$ calibration assumption.

The mathematical framework for the polarimetric calibration of the measured quantities $\mathbf{E'_R}$ and $\mathbf{E'_L}$ can be described in terms of Jones matrices $\mathbf{J}$ [5]

$$\begin{pmatrix} E'_R \\ E'_L \end{pmatrix} = \begin{pmatrix} G_R & 0 \\ 0 & G_L \end{pmatrix} \begin{pmatrix} 1 & D_R \\ D_L & 1 \end{pmatrix} \begin{pmatrix} e^{-i\psi} & 0 \\ 0 & e^{i\psi} \end{pmatrix} \begin{pmatrix} E_R \\ E_L \end{pmatrix} = \mathbf{J} \begin{pmatrix} E_R \\ E_L \end{pmatrix}, \tag{5}$$

where $\mathbf{E_R}$ and $\mathbf{E_L}$ model the true underlying values. Different components of the equation 5 correspond to:

1. field rotation angle ψ, geometric effect related to rotation of polarized component on the sky, known a priori,
2. leakage terms D, parametrizing susceptibility of polarimetric feeds to the perpendicular polarization component, often poorly characterized a priori,
3. gains G, representing scaling of the signal energy related to the sensitivity of telescopes, for which a priori characterization is present, [9], atmospheric variability effects stabilized at the fringe fitting calibration stage [4], and instrumental polarimetric phase offsets, that are relevant for this memo.

From equation 5, combined for a pair of telescopes, we can derive the visibility calibration formula

$$\begin{pmatrix} \mathcal{V}_{RR} & \mathcal{V}_{RL} \\ \mathcal{V}_{LR} & \mathcal{V}_{LL} \end{pmatrix} = \mathbf{V_{12}} = \mathbf{J_1^{-1}}\, \mathbf{V'_{12}}\, (\mathbf{J_2^{-1}})^\dagger = \mathbf{J_1^{-1}}\, (\mathbf{E'_1} \otimes \mathbf{E'^{\dagger}_2})\, (\mathbf{J_2^{-1}})^\dagger = \mathbf{J_1^{-1}} \begin{pmatrix} \mathcal{V}'_{RR} & \mathcal{V}'_{RL} \\ \mathcal{V}'_{LR} & \mathcal{V}'_{LL} \end{pmatrix} (\mathbf{J_2^{-1}})^\dagger, \tag{6}$$

describing the relation between measured visibilities $\mathcal{V}'$ and the true underlying values $\mathcal{V}$.

1.3 Calibration of polarimetric phase gains

The aim of this memo is to describe the calibration of polarimetric phase gains, corresponding to the phase offset between two polarized feeds measured by the telescope. To this end, we assume that field rotation angle ψ, leakage terms D and amplitude components of gains G have been accounted for. In that case equation 5 simplifies to

$$\begin{pmatrix} E'_R \\ E'_L \end{pmatrix} = \begin{pmatrix} 1 & 0 \\ 0 & e^{i\vartheta_{RL}} \end{pmatrix} \begin{pmatrix} E_R \\ E_L \end{pmatrix} = \mathbf{J}_\vartheta \begin{pmatrix} E_R \\ E_L \end{pmatrix}. \tag{7}$$

If additionally we assume absolute calibration of one station (treated here are the first one in the pair), that is $J_{\vartheta,1}$ is an identity matrix, then on baselines to this station we find

$$\begin{pmatrix} \mathcal{V}_{RR} & \mathcal{V}_{RL} \\ \mathcal{V}_{LR} & \mathcal{V}_{LL} \end{pmatrix} = \begin{pmatrix} 1 & 0 \\ 0 & 1 \end{pmatrix}^{-1} \begin{pmatrix} \mathcal{V}'_{RR} & \mathcal{V}'_{RL} \\ \mathcal{V}'_{LR} & \mathcal{V}'_{LL} \end{pmatrix} \left[\begin{pmatrix} 1 & 0 \\ 0 & e^{i\vartheta_{RL,2}} \end{pmatrix}^{-1} \right]^\dagger = \begin{pmatrix} \mathcal{V}'_{RR} & \mathcal{V}'_{RL} \\ \mathcal{V}'_{LR} & \mathcal{V}'_{LL} \end{pmatrix} \begin{pmatrix} 1 & 0 \\ 0 & e^{i\vartheta_{RL,2}} \end{pmatrix}. \tag{8}$$

Under these assumptions the problem reduces to finding a family of phase offsets $\vartheta_{RL,i}$ for all telescopes apart from the absolutely calibrated reference station. We also see that

$$\varepsilon \equiv \arg\left(\frac{\mathcal{V}_{RR}}{\mathcal{V}_{LL}}\right) = \arg\left(\frac{\mathcal{V}'_{RR}}{\mathcal{V}'_{LL}}\right) - \vartheta_{RL,2} = \vartheta'_{RL,2} - \vartheta_{RL,2} \tag{9}$$

and finally

$$\vartheta'_{RL,2} = \vartheta_{RL,2} + \varepsilon. \tag{10}$$

Equation 10 gives a relation between measured phase differences between RR and LL visibilities on baselines to an absolutely calibrated station $\vartheta'_{RL,2}$, instrumental phase offset between the right and left circular polarization receivers on non-calibrated station $\vartheta_{RL,2}$ and unknown true phase difference between RR and LL visibilities ε, expected to be small, $\varepsilon \approx 0$. The Stokes $V = 0$ calibration is tantamount to assuming $\vartheta'_{RL,2} = \vartheta_{RL,2}$. In this work we attempt to disentangle source dependent ε from the instrumental effect ϑ_{RL}.

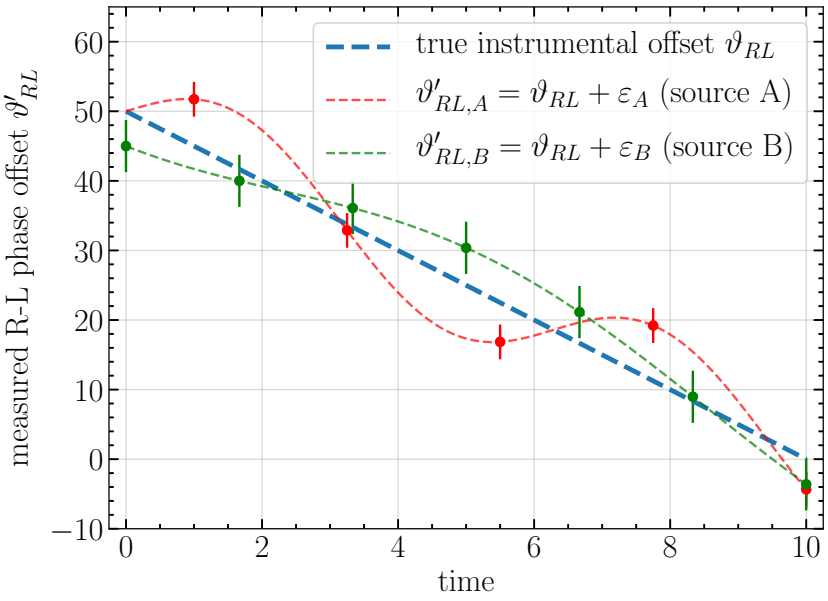

Figure 1: Illustration of the concept of a global in time polarimetric phase gains fit across multiple sources. When using a single source, there is a risk of overfitting to source intrinsic properties (thin dashed lines). This risk can be reduced by using multiple sources.

2 Calibrating polarimetric phase gains

Polarimetric calibration of the EHT data is performed in the framework of the `eat` library [10]. A standard approach to polarimetric phase gains would be to individually treat observations of different sources, calibrating them locally in time to a model of equal mean RR and LL visibility phases. This poses a risk of wiping out signatures of Stokes V by overfitting to source-specific phases ε.

The approach we investigate here is different in two ways:

1. global fits in time are utilized rather than local in time calibration. We can often expect that the instrumental offsets ϑ_{RL} should either be constant in time, or exhibit linear trends,
2. utilizing multiple sources for the calibration to prevent the local overfitting.

A schematic description of this approach is shown in Figure 1. We assume perfect calibration of the ALMA array, and estimate station gain phases on baselines to ALMA within the framework described in Section 1.3. We utilize aggregated data representing multiple observed sources (e.g., the science target source and its calibrators), potentially representing multiple days of an observational campaign. We then fit multiple different models to the data, that is, to the measured phase offsets between RR and LL visibilities on ALMA baselines, $\vartheta'_{RL} = \arg(\mathcal{V}'_{RR}/\mathcal{V}'_{LL})$. The models are fitted utilizing the data thermal uncertainties $\sigma_{\mathrm{th,i}}$ and estimated systematic uncertainties σ_{sys}, with weights

$$w_i = \sigma_i^{-1} = \left(\sigma_{\mathrm{sys}}^2 + \sigma_{\mathrm{th,i}}^2\right)^{-1} . \tag{11}$$

For the presented test we have used $\sigma_{\mathrm{sys}} = 2°$. Models that are fitted to the data fall into two categories:

1. piecewise regression, linear on subdomains, specified number of segments, boundaries between segments are solved for, number of degrees of freedom = 3 × number of segments. Fitted using `mlinsights.mlmodel.PiecewiseRegressor` within the `scikit-learn` framework [11],

2. global polynomials, specified order, number of degrees of freedom = polynomial order +1. Fitted using `numpy.polifit`.

Finally, the optimal model is selected based on an information criterion and added to a calibration text file, utilized by the HOPS-EHT data reduction pipeline [4, 10].

2.1 Information criteria

The two popular methods for optimal model selection are Akaike Information Criterion (AIC, [12]) and Bayesian Information Criterion (BIC, [13]). Formulae governing the criteria are

$$AIC = 2k - 2\ln(\hat{L}), \tag{12}$$

$$BIC = \ln(N)\, k - 2\ln(\hat{L}), \tag{13}$$

in which k represents the number of parameters (degrees of freedom) in the model, N represents the number of datapoints, and $\hat{L}$ is the maximum of the likelihood function for the model. Approximating distributions associated with measurements with normal distributions of known (but different for each datapoint) standard deviation σ_i given by equation 11, we find

$$\ln \hat{L} \approx -\frac{1}{2}\sum_{i=1}^{N}\left(\frac{x_i - m_i}{\sigma_i}\right)^2 + C = -\frac{1}{2}\chi^2 + C. \tag{14}$$

Here x_i is an i-th measurement with uncertainty σ_i, m_i is model prediction for the i-th measurement and C is a model-independent constant. Then, neglecting the constant, the criteria become simply

$$AIC = 2k + \chi^2, \tag{15}$$

$$BIC = \ln(N)\, k + \chi^2. \tag{16}$$

The χ^2 square term is reduced when more degrees of freedom are added to the model. This behavior is counteracted by the term proportional to the number of degrees of freedom k. The optimal model in this framework is simply the one resulting in the smallest value of the information criterion.

We illustrate the model evaluation with the Global Millimeter VLBI Array data from 2017 observation campaign on Galactic Center [14] in Figures 1-3. Baseline connecting ALMA (AA, Chile) and Green Bank Telescope (GB, West Wirginia, USA) is shown.

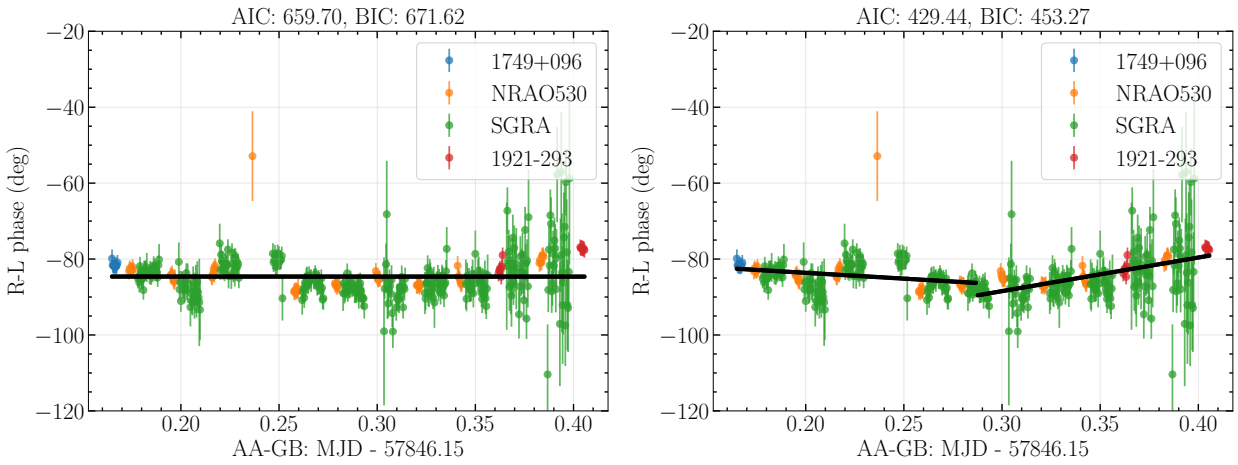

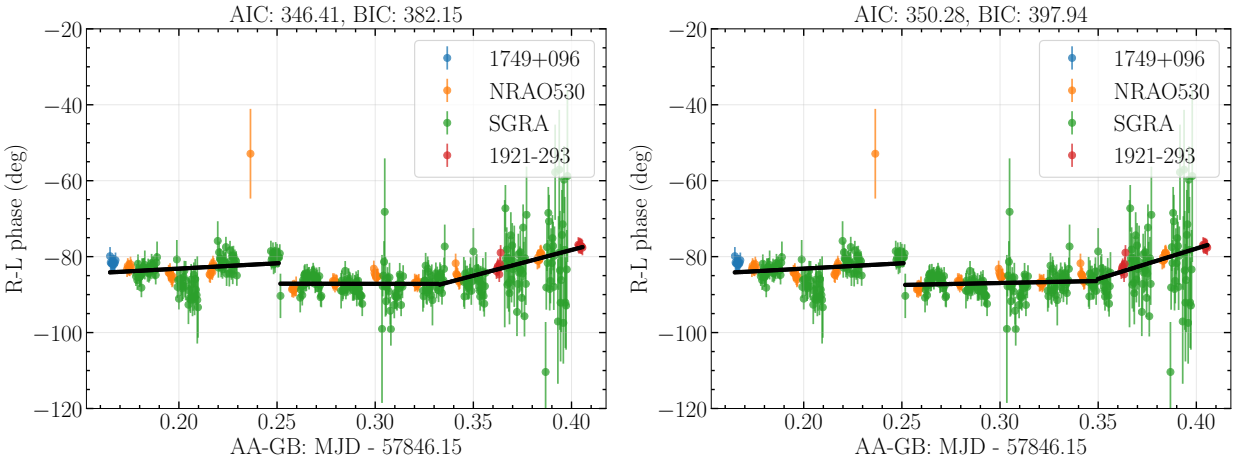

Figure 1: Examples of models with piecewise linear fit with 1,2,3 and 4 segments used. Both criteria favor model with 3 segments (bottom left).

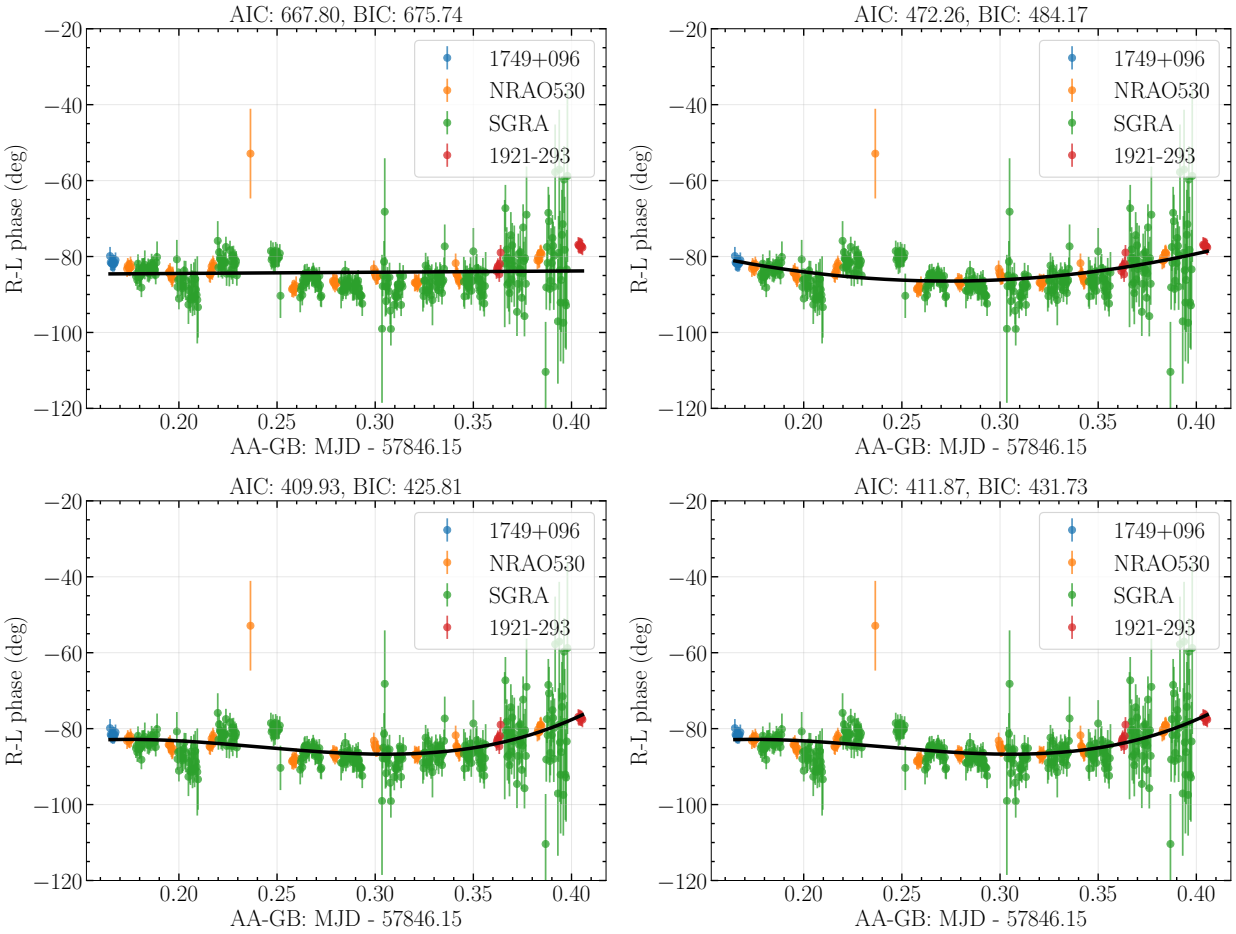

Figure 2: Examples of models with polynomial fit of order 1, 2, 3, 4. Both criteria select third order polynomial (bottom left) as an optimal polynomial degree choice. However, both also point at 3-segments piecewise model as better than any polynomial one.

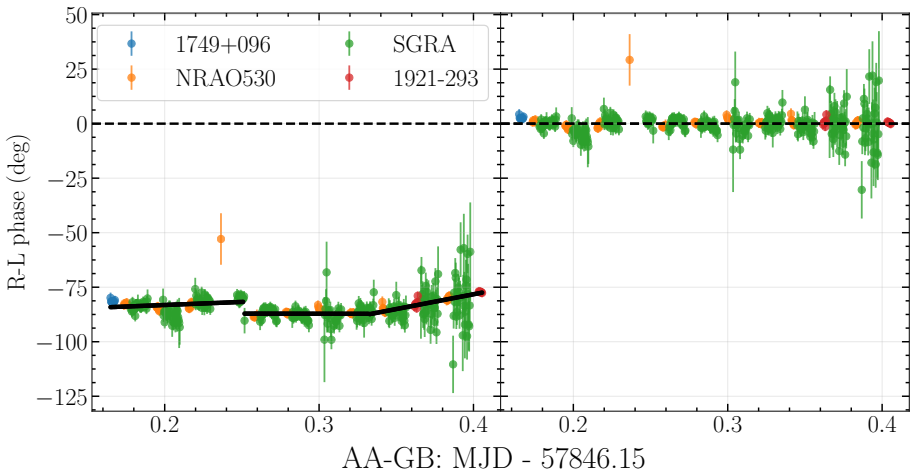

Figure 3: Comparison of R-L phase offsets before and after application of the described calibration procedure.

2.2 Discussion

The method for calibrating instrumental polarimetric phase gains using global in time, multi-source modeling was presented. The method constitutes an alternative to a more standard approach of local in time aligning of right and left circular polarization components phases, and offers a chance to relax the assumptions of the alternative procedure. Because equality between R and L phases is not assumed, data calibrated with this method can be used to obtain more reliable upper limits on the Stokes V component value.

The choice of a particular information criterion is not entirely clear. Both BIC and AIC are the option in the current implementation, and they are often consistent, as in the presented example.

R-L phase offsets could be measured in the future using a tone injection into the recorded data stream. In this way the offsets could be *measured*, rather than *modeled*.

References

[1] A. Richard Thompson, James M. Moran, and George W. Swenson Jr. *Interferometry and Synthesis in Radio Astronomy, 3rd Edition*. Springer International Publishing, 2017.

[2] Jayaram N.Chengalur. Two-element interferometers. `http://www.ncra.tifr.res.in/ncra/gmrt/gmrt-users/low-frequency-radio-astronomy/ch4.pdf`. Online; accessed 11-July-2019.

[3] Event Horizon Telescope Collaboration et al. First M87 Event Horizon Telescope Results. III. Data Processing and Calibration. *ApJL*, 875(1):L3, Apr 2019.

[4] L. Blackburn, C. K. Chan, G. B. Crew, V. L. Fish, S. Issaoun, M. D. Johnson, M. Wielgus, K. Akiyama, J. Barrett, K. L. Bouman, R. Cappallo, A. A. Chael, M. Janssen, C. J. Lonsdale, and S. S. Doeleman. EHT-HOPS Pipeline for Millimeter VLBI Data Reduction. *ApJ*, 882(1):23, Sep 2019.

[5] M. D. Johnson, V. L. Fish, and S. S. Doeleman et al. Resolved magnetic-field structure and variability near the event horizon of Sagittarius A*. *Science*, 350(6265):1242–1245, Dec 2015.

[6] E. Collett. *Field Guide to Polarization*. SPIE Press, 2005.

[7] D. H. Roberts, J. F. C. Wardle, and L. F. Brown. Linear Polarization Radio Imaging at Milliarcsecond Resolution. *ApJ*, 427:718, Jun 1994.

[8] I. Martí-Vidal, A. Roy, J. Conway, and A. J. Zensus. Calibration of mixed-polarization interferometric observations. Tools for the reduction of interferometric data from elements with linear and circular polarization receivers. *A&A*, 587:A143, Mar 2016.

[9] S. Issaoun, T. W. Folkers, L. Blackburn, et al. A conceptual overview of single-dish absolute amplitude calibration. `https://eventhorizontelescope.org/for-astronomers/memos`. EHT Memo 2017-CE-02, Calibration & Error Analysis WG.

[10] L. Blackburn, M. Wielgus, et al. eat library. `https://github.com/sao-eht/eat`. [Online; accessed 30-August-2019].

[11] Fabian Pedregosa, Gaël Varoquaux, Alexandre Gramfort, Vincent Michel, Bertrand Thirion, Olivier Grisel, Mathieu Blondel, Peter Prettenhofer, Ron Weiss, Vincent Dubourg, Jake Vanderplas, Alexandre Passos, David Cournapeau, Matthieu Brucher, Matthieu Perrot, and Édouard Duchesnay. Scikit-learn: Machine learning in python. *J. Mach. Learn. Res.*, 12:2825–2830, November 2011.

[12] Hirotugu Akaike. A new look at the statistical model identification. *Springer Series in Statistics Selected Papers of Hirotugu Akaike*, page 215222, 1974.

[13] Ernst Wit, Edwin Van Den Heuvel, and Jan-Willem Romeijn. 'All models are wrong...': an introduction to model uncertainty. *Statistica Neerlandica*, 66(3):217236, Mar 2012.

[14] S. Issaoun, M. D. Johnson, and L. Blackburn et al. The Size, Shape, and Scattering of Sagittarius A* at 86 GHz: First VLBI with ALMA. *ApJ*, 871(1):30, Jan 2019.